BF2-azadipyrromethene NIR-emissive fluorophores with research and clinical potential.

AUTHOR(S)

Harrison C. Daly, Gonzalo Sampedro, Corentin Bon, Dan Wu, Ghazi Ismail, Ronan A. Cahill, Donal O'Shea

BF_2-Azadipyrromethene NIR-Emissive Fluorophores with Research and Clinical Potential

Harrison C. Daly[a], Gonzalo Sampedro[a], Corentin Bon[a], Dan Wu[a], Ghazi Ismail[b], Ronan A. Cahill[b]*, Donal F. O'Shea[a]*

[a]Department of Medicinal and Pharmaceutical Chemistry, Royal College of Surgeons in Ireland, 123 St. Stephen's Green, Dublin 2, Ireland.

[b]Mater Misericordiae Hospital and School of Medicine, University College Dublin, Belfield, Dublin 4, Ireland.

*Corresponding author

Email address: donalfoshea@rcsi.ie

Abstract

The use of near-infrared fluorescence for *in vivo* research and intraoperative clinical imaging is rapidly expanding, with new applications being proposed and developed. While imaging hardware and software have significantly progressed in recent times, the molecular fluorescent agents remain a limiting factor. In this report, the design, synthesis, photophysical characterization and bio-medical imaging assessment of two new NIR-fluorophores based on the BF_2-azadipyrromethene fluorophore class are described. Inclusion of dimethylamino substituents on these BF_2-azadipyrromethene probes results in very large bathochromic shifts with photophysical measurements showing absorption and emission maxima between 757 and 818 nm within the desired NIR spectra region. Testing of the probes shows that they are suitable for fluorescence imaging with both research and clinical instrumentation. Preclinical imaging assessment shows their suitability as fluorescent markers (tattoos) of lesions for intraoperative identification and lymphatic mapping in *ex vivo* human colonic tissue. These new clinical wavelength-compatible fluorophores may contribute towards the on-going expansion of medical uses for NIR-fluorescence.

Graphical Abstract

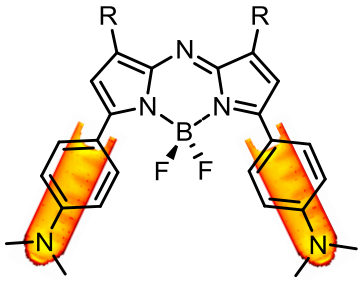

λ_{max} ***flu: 790-820 nm***

Highlights

- NIR-AZA clinical and research imaging
- NIR fluorescent tattoo and lymph node mapping

Key words

NIR-fluorescence; lymph node; tattoo; fluorescence guided surgery

Introduction

The routine use of benign near infrared (NIR) light as a real-time guiding beacon for precision surgery is a concept that is becoming a general clinical reality [1-4]. For this to advance further, several hardware, software and chemical technologies must combine together while seamlessly aligning with the routine of a day-to-day surgical workflow. Over the past decade, significant advances in NIR imaging instrumentation and software have given rise to several clinically used devices [5]. In contrast, advances in NIR-fluorophores remain limited as indocyanine green (ICG) **1** remains the only FDA and EMA clinically approved NIR fluorophore (Figure 1) [6]. In spite of the fact that ICG was first designed for use in photography, clinical approval was granted in the USA in 1959 for hepatic function and cardiac output diagnostics. It is currently clinically used for assessing vascularization following bowel anastomoses [7], reconstructive surgery [8] and for lymph node mapping in the bowel mesentery [9] and breast tissue [10]. Clinical use for imaging of hepatocellular carcinoma has shown the potential wider benefit if NIR-fluorescence could be applied as a general tumour margin delineation technique [11]. Most recently, ICG with NIR imaging has generated excitement for its potential use in precision marking of colorectal cancers, and secondarily as an indicator of draining nodes *via* lymphatic uptake. However, the atypical pharmacokinetics of ICG, which has a half-life of only four minutes and excretion that is exclusively *via* bile, severely limits any further expansion of its clinical uses [12,13].

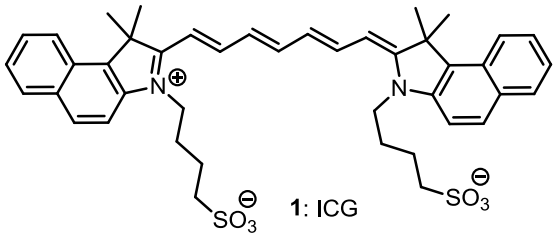

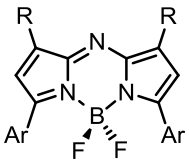

2: R = Me; Ar = 4-$MeOC_6H_4$
λ_{max}: abs 656 nm; emis. 692 nm
3: R = Ph; Ar = 4-$MeOC_6H_4$
λ_{max}: abs 698 nm; emis. 737 nm

Fig. 1. Structure and spectral properties (in DMSO) of ICG **1** and NIR-AZA **2** and **3**.

We have recently embarked on the development of a new class of NIR-fluorophore, namely the BF_2-azadipyrromethene or NIR-AZA class, which has excellent photostability and typical emission wavelengths in the range of 675 to 730 nm (Figure 1) [14-18]. This has been successfully employed in real-time cellular microscopy and small animal imaging but, as yet, suitable longer wavelength derivatives have not been identified for clinical use. To date, this class of fluorophore has shown no cellular or *in vivo* toxicity in the concentration ranges used

for imaging which is a positive indicator for clinical translation [14,16]. In contrast to the NIR-AZA class, ICG has longer wavelengths of absorption and emission at 787 and 818 nm which are preferred for clinical use as deeper light penetration is achievable with these longer wavelengths [19]. A challenge for the development of new clinically useful probes is to closely match these wavelengths such that they are compatible with current clinical instrumentations, which for the most part have fixed wavelengths of excitation tailored to ICG [20]. If substituents could be identified which produced an approximately 100 nm bathochromic emission shift for the NIR-AZA fluorophore class, they would be uniquely placed to provide two distinct emission wavelength sets at ~720 and ~820 nm in the medicinally relevant NIR spectral region. Additionally, once identified, the potential would exist to further structurally elaborate the new derivatives such that they could be bio-conjugated in a similar manner to those previously reported for the 720 nm emitting derivatives [14-16].

Results and Discussion

In this report we discuss our adaption of the NIR-AZA class to have suitable wavelengths that can be utilized with current research and clinical instruments, and make a pre-clinical assessment of imaging performance in human tissue. Several synthetic approaches have been reported to lengthen the wavelength of the NIR-AZA class towards 800 nm by extending conjugation through benzo and hetero fusing aromatic rings to the pyrrole subunits, or by making conformationally restricted derivatives [18,21,22,23]. While these approaches do produce fluorophores of longer wavelengths, they have the disadvantage of requiring lengthy synthetic routes. Our current design employs the use of strong electron donating *p*-dimethylamino substituents on the C-5/5' aryl rings, as shown for target derivatives **4** and **5**, to give the desired bathochromic wavelength shifts (Figure 2).

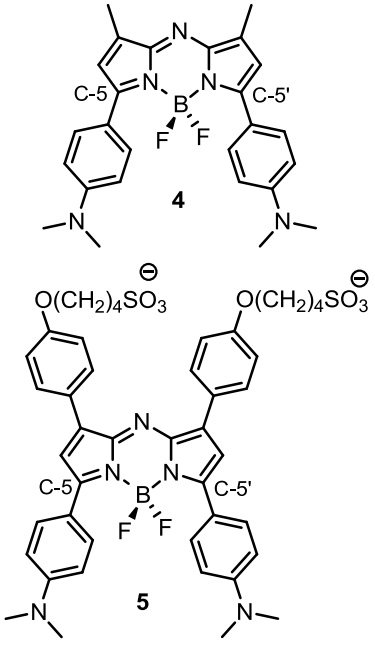

Fig. 2. Structural design of NIR-AZAs **4** and **5**.

Additional alkyl-sulfonic acid groups would be included on **5** to enhance aqueous solubility. While it could be anticipated that a bathochromic shift would be obtained as a result of the inclusion of the amino groups, it was difficult to predict if it would be sufficient to produce the wavelengths required for clinical instrumentation [24]. In addition, whether the emission from **4** or **5** would be visible in tissue was unpredictable as their emissions would most likely be from charge transfer states due to the dimethylamino groups.

The synthetic routes to **4** and **5** intersected at the structurally related unsaturated ketones **6a**, **b**. Compound **6a** was generated from the 1,2-addition of (4-(dimethylamino)phenyl)magnesium bromide to crotonaldehyde with subsequent oxidation and **6b** from condensation of 1-(4-(dimethylamino)phenyl)ethanone with 4-hydroxybenzaldehyde. Addition of nitromethane gave **7a**,**b** which upon heating with ammonium acetate in alcohol gave **8a**,**b**. Conversion to BF_2 chelates was achieved at room temperature in CH_2Cl_2, to give the targeted fluorophore **4** and the penultimate compound **9**. Reaction of **9** with 1,2-oxathiane 2,2-dioxide in THF under reflux gave the bis-alkyl sulfonic acid substituted fluorophore **5**.

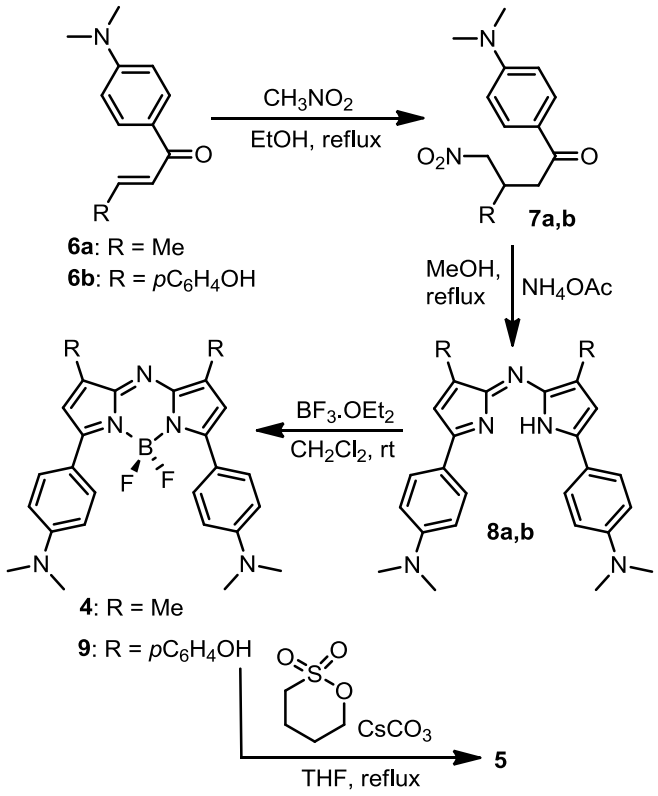

Scheme 1. Synthetic routes to NIR-fluorophores **4** and **5**.

All synthetized compounds were purified by chromatography and characterized by nuclear magnetic resonance (^1H, ^{13}C) and mass spectrometry. In addition, single crystals of **9** were grown from CH_2Cl_2/hexane and one used for X-ray crystallographic analysis to confirm the molecular structure and overall conjugated nature of the chromophore **9** (Figure 3). Evidence for a strong delocalization from the aniline nitrogens into the chromophore system was

apparent from the relatively short N-C bond lengths for N(3)-C(4) and N(41)-C(38) at 1.355(5) Å and 1.374(6) Å respectively and the small torsion angles for C(1)-N(3)-C(4)-C(5) and C(42)-N(41)-C(38)-C(37) of 11.9(6)° and 14.5(6)°. This delocalization would be the primary contributor to extending absorption and emission to longer wavelengths.

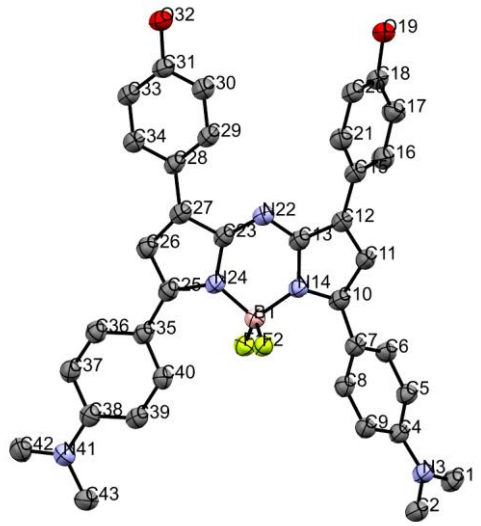

Fig. 3. X-Ray crystal structure of **9** with thermal ellipsoids drawn at 50% probability level. Hydrogens and co-crystallised molecules of water and CH_2Cl_2 omitted for clarity.

Spectroscopic analysis of **4**, **9** and **5** was carried out in a selection of organic media (DMSO, THF, toluene) and aqueous media. Encouragingly, **4** showed promising absorption and fluorescence characteristics in both polar and non-polar solvents (Table 1). For example, in DMSO the changing of *p*-OMe groups of **2** to the *p*-$N(CH_3)_2$ groups of **4** gave rise to remarkable bathochromic shifts of 118 and 130 nm for absorption and emission maxima respectively (entries 1 and 2). Wavelengths of **4** in DMSO were also encouraging with 774 and 822 nm being the observed λ max values, which are comparable to literature values for ICG of 787 and 818 nm (entry 2) [19]. In less polar solvents such as THF, abs/emis were recorded at 744 and 791 nm respectively with non-polar toluene slightly further blue shifted (entries 3 and 4). Fluorescence quantum yield showed solvent dependence and was highest in toluene (0.21) and THF (0.13) and lower in DMSO (0.01) (Table 1). As fluorophore **5** had limited solubility in organic solvents, the properties of **9** were first examined (entries 5-7). As expected, the inclusion of two additional aromatic ring substituents further lengthened the absorbance and emission maxima when compared to **4** with, for example, abs and flu maxima at 794 and 832 nm in DMSO (entry 6). A slight reduction in fluorescence quantum yields in comparison to **4** was also recorded with the highest value in toluene of 0.1 (entry 7). Analysis of the bis-sulfonic acid substituted fluorophore **5** in DMSO gave promising absorption and emission maximia of 786 and 826 nm respectively, though with a low quantum yield (Table 1, entry 8).

Table 1. Absorbance and emission spectra of **2** (black) and **4** (red) in DMSO with spectroscopic parameters for **2**, **4, 5** and **9**.

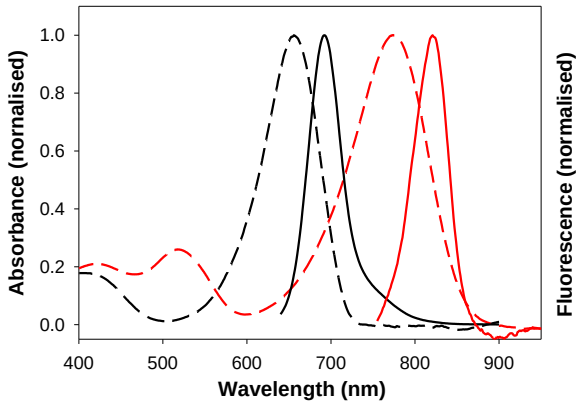

Entry	Compound	Solvent	λ_{max} abs (nm)	FWHM	λ_{max} flu (nm)	Stokes Shift (nm)	ϕflu
1	**2**	DMSO	656	78	692	36	0.44[a]
2	**4**	DMSO	774	107	822	48	0.01
3	**4**	THF	744	94	791	47	0.13
4	**4**	toluene	734	92	779	45	0.21
5	**9**	DMSO	794	108	832	38	>0.01
6	**9**	THF	775	96	815	40	0.04
7	**9**	toluene	778	97	813	35	0.10
8	**5**	DMSO	786	103	826	40	>0.01

[a] Value reported in $CHCl_3$ [17].

In pure aqueous media, ICG **1** and fluorophores **4** and **5** showed complex spectra due to complex aggregates so 1% aqueous Kolliphor EL buffer solutions at pH 7 of each were used to allow their properties to be investigated and compared [25]. Kolliphor EL is a clinically approved agent used for the delivery of water insoluble drugs such as cyclosporine A, diazepam and paclitaxel [26]. ICG solutions gave absorption and emission maxima at 794 and 818 nm, close to literature reported values in water (Table 2, entry 1) [25]. We were pleased to find that our new fluorophores **4** and **5** showed similar spectral properties. While absorption for **4** was blue shifted by 37 nm relative to **1**, emission maxima was only 29 nm shorted due to its larger Stokes shift (entry 2). Absorption of fluorophore **5** was marginally red shifted by 4 nm at 798 nm relative to ICG and had emission maxima identical to ICG at 818 nm (entry 3). Using the quantum yield of ICG in DMSO as a reference, its quantum yield in this aqueous solution was measured to be 7%. In comparison, quantum yields for **4** and **5** were measured at 9% and 3% respectively, indicating that they would be suitable for use with small animal and clinical imaging systems. Comparative photobleaching experiments for **1, 4** and **5** in phenol red free Dulbecco's modified eagle's medium (iDMEM) showed over 90% loss of fluorescence for **1** with less than 10% loss for **4** and **5** after 30 min irradiation, confirming their superiour stability (Table 2).

Table 2. Comparison of aqueous spectral and photo-bleaching properties of **1**, **4** and **5**.[a,b]

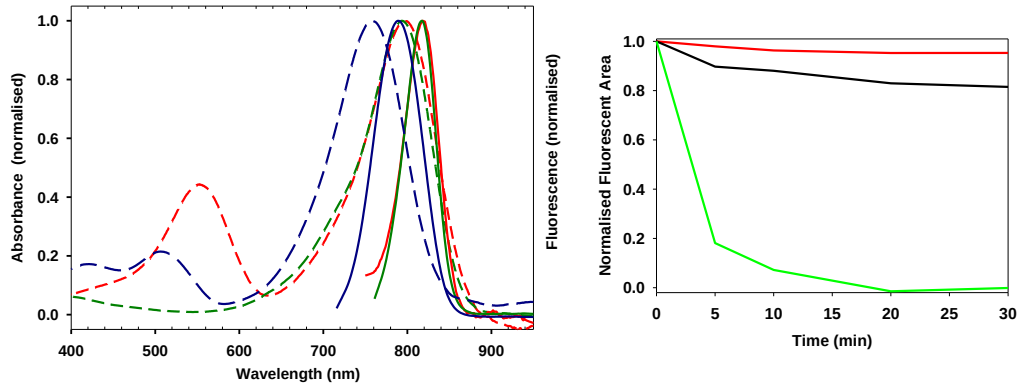

Entry	Fluorophore	λ_{max} abs (nm)	FWHM	λ_{max} flu (nm)	Stokes Shift (nm)	ϕ_{flu} [c]
1	**1**	794	93	818	24	0.07
2	**4**	757	101	789	32	0.09
3	**5**	798	105	818	20	0.03

[a]Left: Absorption and emission spectra of **1** (green traces); **4** (blue traces); **5** (red traces) in 1% aqueous Kolliphor EL buffer solutions. [b]Right: Comparative photo-bleaching of **1** (green trace); **4** (blue trace); **5** (red trace) in iDMEM 1% aqueous Kolliphor EL buffer. [c]Relative to **1** in DMSO [19].

The sensitivity and stability of the emission properties of **4** and **5** were tested to determine if they were susceptible to change across the pH range as this is an important parameter that must be considered for *in vivo* imaging [27]. pH titrations showed negligible difference in emission intensities between pH 8 and 4 for both fluorophores and only upon reaching pH 3 did the emission intensities reduced (Figure 4, panel A and SI).

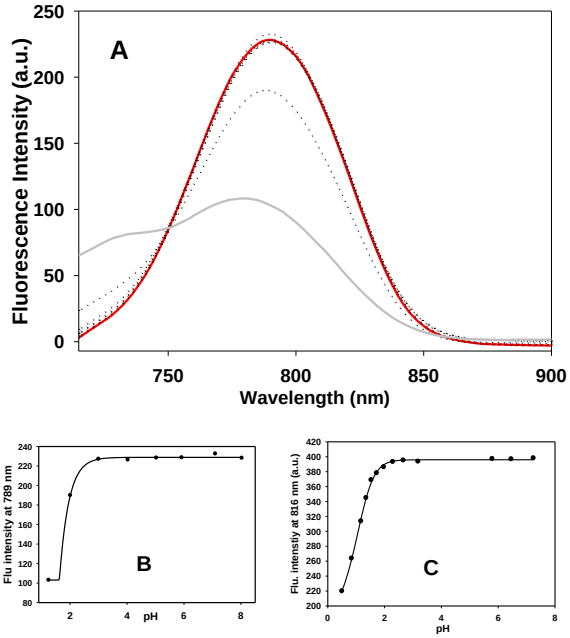

Fig 4. Panel A: Emission spectra of **4** in the pH range of 1 - 8. Panel B: Plot of pH versus emission intensity for **4** giving pKa value of 1.6. Panel C: Plot of pH versus emission intensity for **5** giving pKa value of 1.3.

pKa values for aniline protonation for **4** and **5** measured as 1.6 and 1.3 respectively which are well beyond any biological levels of acidity. In addition, solutions of 4 and 5 were maintained at either pH 4 or 8 for 24 hours showed negligible variation in emission intensities or wavelengths.

Next the imaging performance of 5 μM solutions of **1**, **4** and **5** was assessed using the IVIS spectrum research imaging system. Images were recorded using an excitation wavelength of 745(30) nm and with three different emission filter settings of 800(20), 820(20), and 840(20) nm (Figure 5). Fluorophore **4** was clearly the brightest of the three fluorophores at 800(20) nm and was comparable with **1** with both 820(20) and 840(20) filters (Figure 5, graph). The fluorescence intensity from **5** was lowest of the three derivatives, which is in agreement with quantum yield values. A similar trend of emission intensities was seen for solutions at 10 μM concentration. Overall, it can be concluded that NIR-fluorophores **4** and **5** are employable with research and clinically used instruments.

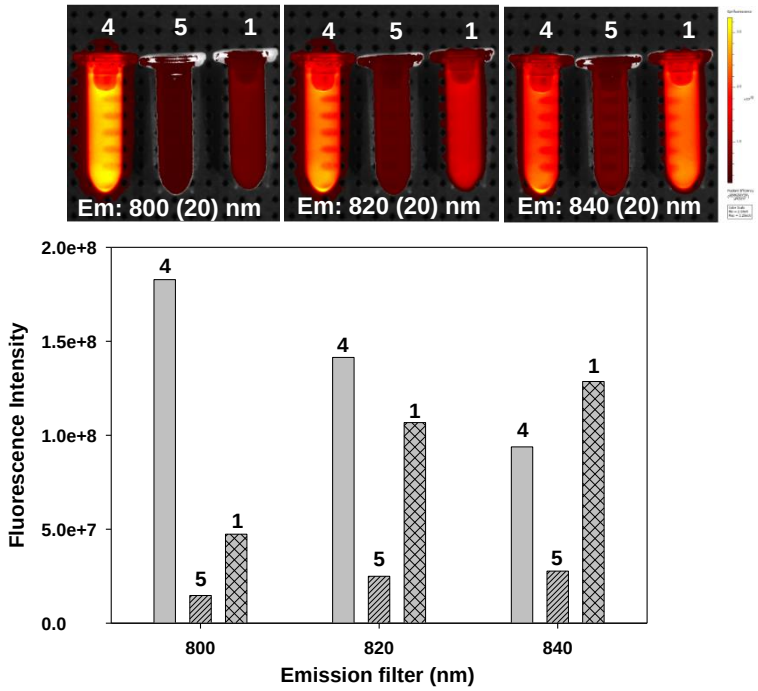

Fig. 5. Top: IVIS spectrum images of 5 μM solutions of **1**, **4**, and **5** with varying emission filters (excit at 745(30) nm). Bottom: Plot of eppendorf fluorescence intensity using different emission filters of 800 (20), 820(20) and 840 (20) nm.

The Novadaq PINPOINT Endoscopic system is one of the more common clinically used instruments for fluorescence guided surgery with ICG. It utilises the longest excitation wavelength of any clinical instrument at 806 nm, making it a particularly challenging device for alternative fluorophores [5]. Encouragingly, the imaging of 10 μM aqueous buffered solutions of **1**, **4**, and **5** showed all three to be strongly fluorescent with qualitatively **1** being marginally brighter which would be in keeping with the spectroscopic characteristics described above (Figure 6, panel A).

Endoscopic tattooing is a commonly used method in gastroenterology and colorectal surgeries, facilitating the identification of previously detected anomalies or lesions during surgery. Typically, this is done using the non-fluorescent dye India ink though it suffers from an approximate 10% failure rate in part due to its faintness and its poor visibility in patients with increased body mass index [28]. This problem risks prolongation of operation, change of surgical procedure (including conversion to laparotomy) and increases the risk of wrong site surgery as well as necessitating additional intraoperative manoeuvres such as complete colonic inspection and on table colonoscopy. With an increasing proportion of tumors now being identified through general population screening as small sized or early stage, the need for their exact localization during surgery is an increasingly under-met clinical need. The potential clinical advantages of using alternative NIR fluorescent markers for increasing perioperative precision has been recognised but remains as of yet undeveloped [29].
As such, emissions of **1**, **4** and **5** were compared as fluorescent tattoos following submucosal injection of 0.1 mL of 10 μM solutions in *ex vivo* colonic tissue, with visualization using the Novadaq system (Figure 6, panel B).

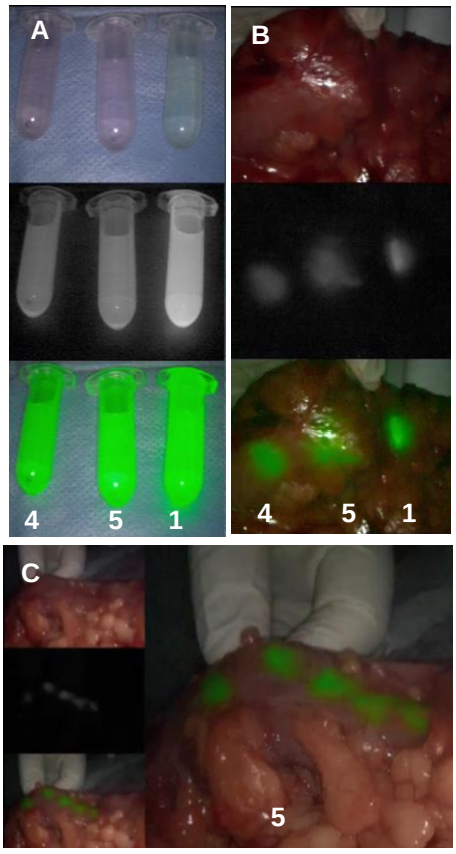

Fig. 6. Imaging with Novadaq PINPOINT Endoscopic instrument. Panel A: 10 μM solutions of **4**, **5** and **1** viewed as white light video (top), NIR fluorescence, shown in grey-scale, (middle) and overlay of NIR fluorescence, shown in green, and white light video (bottom). Panel B: Injection site of 0.1 mL of a 10 μM solutions of **4**, **5** and **1** in *ex vivo* colonic tissue as viewed in white light video (top), NIR fluorescence, shown in grey-scale, (middle) and overlay of NIR-fluorescence, shown in green, and white light video (bottom). Panel C: Five individual tattoos using 0.1 mL injections of 10 μM solution of **5.**

At these low concentrations, no colouration at the injection sites was observed in the white light camera view yet each tattoo could be readily visualised in NIR-fluorescent mode. It was noted that tattoos from **4** or **5** did not dissipate or spread out from their point of injection, which may offer advantage when precision marking is required. This was confirmed by making five individual tattoos using 0.1 mL injections of **5** (10 μM) within 10 cm of tissue, which remained individually distinct and did not merge together (Figure 6, panel C).

Lymph node detection and staging is the most important prognostic factor contributing to colorectal cancer patient treatment planning and as such, clinical NIR-fluorescent lymphatic mapping is an increasingly utilised intraoperative procedure [9, 30]. The ability for regional lymphatic mapping based on the patients individual anatomy is increasingly viewed as an important next step advance in surgical practice most especially in conjunction with tailored cancer-specific probes which could allow discrimination between malignant and benign disease at the time of operation and aid in the move towards tailored operative extent based on patient disease specifics rather than general probabilities and standard anatomic expectations [31]. In a recent report it has been shown that lymph node mapping in *ex vivo* resected colonic tissue is a useful experimental method for pre-clinical assessment of NIR-fluorophores [32]. Using this approach, tissue specimens obtained from surgical procedures in the Mater Misericordiae University hospital were used for imaging experiments as soon as possible following resection, such that it did not interfere with the ongoing surgical procedure (within 30-60 mins after removal). To illustrate the potential for lymph node mapping with **4**, 1 mL of a 10 μM solution was injected close to the tumour mass from which migration through the lymphatics to distant lymph nodes was observed (Figure 7).

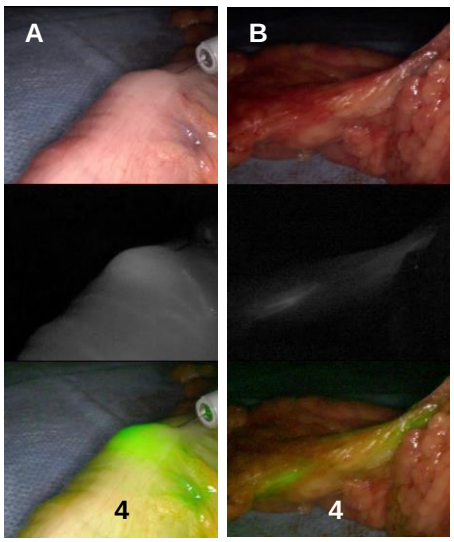

Fig. 7. *Ex vivo* human colonic tissue imaging. Panel A: injection site of **4** (1 mL, 10 μM) viewed as white light video (top), NIR fluorescence, shown in grey-scale (middle) and overlay of NIR-fluorescence, shown in green, and white light video (bottom). Panel B: Lymphatic imaging distant from injection site as viewed in white light video (top), NIR fluorescence shown in grey-scale (middle) and overlay of BIR-fluorescence, shown in green, and white light video (bottom).

Upon injection of **4**, both the primary site of injection and the immediate surrounding lymphatic channels became fluorescent (Figure 7; panel A). Soon afterwards, sites over 10 cm distant from the position of injection showed areas of localised fluorescence in tissue regions containing lymph nodes (Figure 7, panel B) [33]. Subsequent histological examination showed no toxic local effects of the fluorophore on the surrounding tissue. These demonstrations of NIR-fluorescent lymphatic mapping and tissue tattooing highlight the future clinical potential of **4** and **5** as intraoperative guides to complex surgical procedures.

Conclusion

In this study we report the straight forward synthesis of two novel dimethyl-amino substituted NIR-AZA fluorophores **4** and **5** with photophysical properties in the spectral region required for small animal research and clinical use. Preliminary assessments with commonly used research and clinical instrumentation clearly illustrate their suitability for use with these imaging devices. Positive fluorescent tattooing and lymphatic imaging results in *ex vivo* human colonic tissue specimens show, for the first time, the clinical potential of the NIR-AZA fluorophore class. This proof-of-concept study illustrates how dimethylamino substitution of NIR-AZA fluorophores can provide the spectral wavelengths from which new medical and surgical imaging procedures may emerge.

Experimental Protocols

General

All commercially available solvents and reagents were used as supplied. Gel chromatography was performed with Davisil 60 silica (230-400 mesh) and visualised on Merck millipore TLC silica gel 60 F_{254} plates. On the basis of NMR and reverse phase HPLC, final compounds were >95% pure. ^{1}H and ^{13}C spectra were recorded on 400 MHz Bruker NMR spectrometer and chemical shifts were reported in ppm using solvent residual peaks as standard. Low resolution mass spectrometry was carried out on an Advion Expression CMS instrument. High resolution mass spectrometry was performed by on a Quattro Micro™ liquid chromatography instrument or on a Waters LCT Premier (LC and ToF) instrument. Melting points were measured using a Gallenkamp melting point apparatus. Analytical reverse phase HPLC was carried out using a Shimadzu Prominence LC system using YMC- Triart Phenyl column 150mm x 4.6 mm I.D. S - 5µm, 12nm. Absorbance spectra were recorded with a Varian Cary 50 Scan UV-Visible Spectrophotometer. Fluorescence spectra were recorded with a Varian Cary Eclipse Fluorescence Spectrophotometer. Organic solvents for absorbance and fluorescence experiments were of HPLC quality and milipore filter HPLC grade water was used. SigmaPlot, MestreNova, ChemDraw and Living Image software were used for data analysis. Imaging experiments conducting using an IVIS spectrum noninvasive quantitative molecular imaging system from Caliper Life Sciences and a Pinpoint endoscopic fluorescence imaging system from Novadaq Technologies.

Chemistry

Synthesis of 1-(4-(dimethylamino)phenyl-3-methyl-4-nitrobutan-1-one 7a.

Mg turnings (0.97 g, 3.99 mmol) and two crystals of I_2 in anhydrous THF at rt were treated with 4-bromo-*N*,*N*-dimethylaniline (5 mL of a 0.5 M THF solution) and heated under reflux. Once reaction had initiated additional 4-bromo-*N*,*N*-dimethylaniline (6.67 g, 3.33 mmol, 73 mL anhydrous THF) was added slowly over 15 minutes following which the reaction mixture was heated under reflux for 4 h. The reaction was cooled to rt and added slowly to a solution of crotonaldehyde (2.51 mL, 3.03 mmol) at 0 °C in anhydrous THF (13 mL). Following addition, the reaction mixture was stirred at rt for 2 h, quenched with NH_4Cl (50 mL) and H_2O (100 mL) added. Reaction mixture was extracted with EtOAc (3 × 100 mL), washed with brine (100 mL), dried over Na_2SO_4, filtered and reduced to dryness *in vacuo* to give 1-(4-(dimethylamino)phenyl)but-2-en-1-ol (6.16 g) as a yellow oil. This oil was dissolved in anhydrous 1,4 dioxane (130 mL, 0.25 M), treated with sequential addition of 2,3-dichloro-5,6-dicyanobenzoquinone (8 g, 3.52 mmol). After stirring at rt for 3 h the reaction mixture was filtered through a pad of celite and eluted with EtOAc (100 mL). The celite was suspended in EtOAc (50 mL) and filtered with this process being repeated until no more crude product was seen visualised by TLC. The organic fractions were combined and reduced to dryness *in vacuo* to afford crude **6a** (6.16 g). Without further purification, **6a** was dissolved in EtOH (200 mL), treated with diethylamine (33 mL, 3.25 mmol), nitromethane (17.6 mL, 3.25 mmol) and heated under reflux for 24 h. The reaction mixture was cooled, reduced to dryness *in vacuo*, treated with H_2O (200 mL) and EtOAc (200 mL). Following separation the aqueous phase was extracted with EtOAc (100 mL), the organic fractions were combined, washed with brine (3 × 100 mL), dried over Na_2SO_4, filtered and reduced to dryness *in vacuo* to give the crude product as a brown oil. Product was purified by silica gel chromatography (10:1 to 5:1; cyclohexane: EtOAc) to afford **7a** as a light brown solid, mp 54-57 °C (4.26g, 51%). ^{1}H NMR (400 MHz, $CDCl_3$): δ 7.86 (d, *J* = 9.1 Hz, 2H), 6.66 (d, *J* = 9.1 Hz, 2H), 4.71 – 4.25 (m, 2H), 3.07 (s, *J* = 4.1 Hz, 6H), 3.05 – 2.83 (m, 3H), 1.13 (d, *J* = 6.7 Hz, 3H) ppm. ^{13}C NMR (100 MHz, $CDCl_3$): δ 195.7, 153.8, 130.4, 124.9, 110.9, 81.0, 41.2, 40.2, 29.3, 17.8 ppm. HRMS (TOF MS ES+) m/z: $[M + H]^+$ Calcd. for $C_{13}H_{19}N_2O_3$ 251.1396; Found 251.1395.

Synthesis of (*E*)-1-(4-(dimethylamino)phenyl)-3-(4-hydroxyphenyl)prop-2-en-1-one 6b.

4-*N*,*N*-Dimethylaminoacetophenone (5.0 g, 30.6 mmol) and 4-hydroxybenzaldehyde (4.6 g, 37.7 mmol) in EtOH (50 mL) were treated with aqueous NaOH (40 mL, 4.0 mmol) and heated under reflux for 24 h. During the course of the reaction the product precipitated from the reaction mixture. After cooling, the reaction mixture was adjusted to pH 7, filtered and the precipitate washed with hot water to give the product **6b** as a yellow solid, mp 116-118 °C (7.1 g, 74%). ^{1}H NMR (400 MHz, DMSO-d_6) δ: 10.00 (s, 1H), 8.02 (d, *J* = 9.0 Hz, 2H), 7.73 – 7.66 (m, 3H), 7.57 (d, *J* = 15.4 Hz, 1H), 6.82 (d, *J* = 8.5 Hz, 2H), 6.75 (d, *J* = 9.0 Hz, 2H), 3.03 (s, 6H) ppm. ^{13}C NMR (100 MHz, DMSO-d_6) δ: 186.1, 159.6, 153.2, 142.1, 130.6, 130.5, 126.2, 125.5, 118.8, 115.7, 110.8, 39.7 ppm. MS (ESI+) m/z: $[M+H]^+$ Calcd. for $C_{17}H_{18}NO_2$ 268.3; Found 268.1.

Synthesis of 1-(4-(dimethylamino)phenyl)-3-(4-hydroxyphenyl)-4-nitrobutan-1-one 7b.

A solution of **6b** (3.75 g, 14 mmol), nitromethane (15 mL, 140 mmol) and diethylamine (9 mL,140 mmol) in MeOH (100 mL) was heated under reflux for 24 h. After cooling to rt, the solvent was removed *in vacuo* and the residue obtained dissolved in water (50 mL), neutralized with HCl 4 M and extracted with ethyl acetate (3 × 100 mL). The combined

organic layers were washed with water (3 × 50 mL) dried over Na_2SO_4 and concentrated to dryness yielding the product **7b** as a yellow solid, mp 114-116 °C (3.5 g, 78%). ^{1}H NMR (400 MHz, DMSO-*d*$_6$) δ: 9.31 (s, 1H), 7.76 (d, *J* = 9.0 Hz, 2H), 7.13 (d, *J* = 8.5 Hz, 2H), 6.67 (t, *J* = 9.5 Hz, 4H), 4.83 (ddd, *J* = 22.4, 12.6, 7.8 Hz, 2H), 3.98 – 3.85 (m, 1H), 3.37 – 3.12 (m, 2H), 2.99 (s, Hz, 6H) ppm. ^{13}C NMR (100 MHz, DMSO-d_6) δ: 194.7, 156.4, 153.3, 130.2, 123.0, 128.7, 124.1, 115.2, 110.6, 80.2, 40.4, 39.6, 39.1 ppm. MS (ESI+) m/z: $[M + Na]^+$ Calcd. for $C_{18}H_{20}N_2O_4Na$ 351.3; Found 351.3.

Synthesis of (*Z*)-4-(5-(4-(dimethylamino)phenyl)-2-((5-(4-(dimethylamino)phenyl)-3-(4-hydroxyphenyl)-*1H*-pyrrol-2-yl)imino)-*2H*-pyrrol-3-yl)phenol 8b.

A solution of **7b** (7.8 g, 24 mmol) and NH_4OAc (67.7 g, 870 mmol) in EtOH (100 mL) was heated under reflux for 24 h. After cooling to rt, the solvent was concentrated to a quarter of its original volume, cooled in an ice bath for 1 h. The resulting precipitate was filtered, and washed with cold EtOH to yield the product **8b** as a dark solid, mp 240-242 °C (5.4 g, 40 %). ^{1}H NMR (400 MHz, DMSO-*d*$_6$) δ: 7.96 (d, *J* = 8.6 Hz, 4H), 7.87 (d, *J* = 9.0 Hz, 4H), 7.31 (s, 2H), 6.93 (d, *J* = 9.0 Hz, 4H), 6.83 (d, *J* = 8.6 Hz, 4H), 3.07 (s, 12H) ppm. ^{13}C NMR (100 MHz, DMSO-*d*$_6$) δ: 172.1, 157.4, 153.2, 151.4, 148.3, 140.2, 129.9, 127.6, 125.0, 118.9, 115.1, 112.5 ppm. (Aniline peak masked by solvent signal). MS (ESI−) m/z: $[M-H]^-$ Calcd. for $C_{36}H_{32}N_5O_2$ 566.7; Found 566.5.

Synthesis of 3,7-bis(4-(dimethylamino)phenyl)-5,5-difluoro-1,9-bis(4-hydroxyphenyl)-*5H*-dipyrrolo[1,2-c:2',1'-f][1,3,5,2]triazaborinin-4-ium-5-uide 9.

A solution of **8b** (1 g, 1.8 mmol) and diisopropylethylamine (3.2 mL g, 18 mmol) in CH_2Cl_2 (50 mL) was stirred for 15 min cooled to 0 °C, treated dropwise with $BF_3.Et_2O$ (4 mL, 32 mmol) and stirred under N_2 for 24 h. The reaction mixture was diluted with DCM (30 mL), washed with water (100 mL) and the organic layer evaporated do dryness. Purification by short column chromatography on silica eluting with CH_2Cl_2/MeOH (4:1) gave **9** as a purple solid, mp > 300 °C (1 g, 93 %). ^{1}H NMR (400 MHz, DMSO-*d*$_6$) δ: 10.26 (s, 2H), 8.11 (d, *J* = 8.5 Hz, 4H), 7.99 (d, *J* = 8.5 Hz, 4H), 7.19 (s, 2H), 6.91 (d, *J* = 8.5 Hz, 4H), 6.83 (d, *J* = 8.7 Hz, 4H), 3.02 (s, 12H) ppm. ^{13}C NMR (100 MHz, DMSO-*d*$_6$) δ: 160.0, 155.9, 151.0, 144.1, 141.8, 131.4, 130.4, 122.6, 120.1, 115.6, 114.8, 112.0, 39.8 ppm. HRMS (TOF MS LD+) m/z: $[M]^+$ Calcd. for $C_{36}H_{32}BN_5O_2F_2$ 615.2617; Found 615.2678.

Synthesis of the BF_2 Chelate of (Z)-4-(4-(5-(4-(dimethylamino)phenyl)-2-((5-(4-(dimethylamino)phenyl)-3-(4-(4-sulfonatobutoxy)phenyl)-*1H*-pyrrol-2-yl)imino)-*2H*-pyrrol-3-yl)phenoxy)butane-1-sulfonate 5.

Compound **9** (100 mg 0.16 mmol) and dry $CsCO_3$ (260g, 0.8 mmol) in dry THF (5 mL) under N_2 were treated and 1,2-oxathiane 2,2-dioxide (80 μL, 0.8 mmol) and the reaction mixture heated under reflux for 16 h. The mixture was cooled to rt and the solvent removed *in vacuo*. EtOAc (10 mL) was added and the resulting solid suspension filtered and washed with EtOAc (3×10 mL). Purification using Sephadex G-25 column eluting with water with isolation by freeze drying gave the product **5** as a purple solid, mp >300 °C (113 mg, 80%). ^{1}H NMR (400 MHz, DMSO-*d*$_6$) δ: 8.13 (d, *J* = 9.0 Hz, 4H), 8.06 (d, *J* = 9.0 Hz, 4H), 7.25 (s, 2H), 7.08 (d, *J* = 9.0 Hz, 4H), 6.86 (d, *J* = 9.0 Hz, 4H), 4.08 (t, *J* = 6.2 Hz, 4H), 3.06 (s, 12H), 1.89 – 1.67 (m, 8H) ppm. (2×CH_2 peaks masked by solvent peaks). ^{13}C NMR (100 MHz, DMSO-*d*$_6$) δ: 160.7, 155.8, 151.1, 144.2, 142.0, 131.2, 130.5, 123.8, 120.0, 115.0, 114.6,

112.1, 67.7, 51.1, 39.8, 28.0, 21.9 ppm. (Aniline peak masked by solvent peaks). HRMS (TOF MS LD-) m/z: $[M-H]^-$ Calcd. for $C_{44}H_{47}BF_2N_5O_8S_2$ 886.2927; Found 886.2892.

Synthesis of 3,7-bis(4-(dimethylamino)phenyl)-5,5-difluoro-1,9-dimethyl-5H-dipyrrolo[1,2-c:2',1'-f][1,3,5,2]triazaborinin-4-ium-5-uide 4.

A solution of **7a** (4.2 g, 16.8 mmol) in MeOH (60 mL, 0.28 M) was treated with NH_4OAc (47.8 g, 0.62 mol) and heated under reflux for 10 h. The reaction mixture was cooled in a NaCl-ice bath, the resulting precipitate was filtered and washed with ice cold MeOH (10 mL). The precipitate was suspended in saturated $NaHCO_3$ (3×60 mL) and filtered followed by suspension in H_2O (3×60 mL) and filtration. The collected product was dried under vacuum to give **8a** as a dark solid (1.19 g, 35%). Without further purification, **8a** (1g, 2.4 mmol) was dissolved in anhydrous CH_2Cl_2 (245 mL), treated with diisopropylethylamine (4.25 mL, 24.3 mmol) and stirred for 15 mins. The solution was cooled in an ice bath, $BF_3.OC_4H_{10}$ (4.2 mL, 34.1 mmol) added dropwise and the reaction stirred at rt for 16 h under N_2. Reaction solvent was reduced to dryness *in vacuo*, the residue dissolved in EtOAc (200 mL) and saturated Na_2CO_3 (100 mL) added. The organic phase was separated, washed with H_2O (2×100 mL) and brine (100 mL) and reduced to dryness *in vacuo*. The residue was purified by silica gel chromatography (99:1; CH_2Cl_2: EtOAc) to afford **4** as a green metallic solid, mp >200 °C (403 mg, 36%). ^{1}H NMR (400 MHz, $CDCl_3$) δ: 8.13 – 7.94 (m, 4H), 6.80 – 6.68 (m, 4H), 6.65 (s, *J* = 8.2 Hz, 2H), 3.06 (s, 12H), 2.33 (s, 6H) ppm. ^{13}C NMR (100 MHz, $CDCl_3$) δ: 156.6, 151.7, 146.2, 140.8, 131.5 (t, *J* = 5.3 Hz), 120.5, 119.5, 111.9, 40.2, 11.3. ^{19}F NMR (376 MHz, $CDCl_3$) δ -133.71 (dd, *J* = 66.6, 33.3 Hz) ppm. HRMS (TOF MS ES+) m/z: $[M]^+$ Calcd. for $C_{26}H_{28}BF_2N_5$ 495.2406; Found 459.2384.

Crystallography

A single crystal of **9**, grown from CH_2Cl_2/hexane of approximate dimensions 0.020 mm x 0.040 mm x 0.210 mm, was used for the X-ray crystallographic analysis. The X-ray intensity data were measured at 100(2)K using an Oxford Cryosystems low temperature device using a MiTeGen micromount. Bruker APEX software was used to correct for Lorentz and polarization effects. A total of 1649 frames were collected. The integration of the data using a triclinic unit cell yielded a total of 17578 reflections to a maximum θ angle of 68.31 (0.83 Å resolution), of which 5748 were independent (average redundancy 3.058, completeness = 98.9%, R_{int} = 7.76%, R_{sig} = 11.34%) and 3685 (64.11%) were greater than $2\sigma(F^2)$. The final cell constants of a = 10.0085(6) Å, b = 12.0655(6) Å, c = 13.6633(8) Å, α = 78.198(4), β = 80.668(4), γ = 81.735(4), volume = 1583.21(16) $Å^3$, are based upon the refinement of the XYZ-centroids of reflections above 20 σ(I). Data were corrected for absorption effects using the Multi-Scan method (SADABS). The ratio of minimum to maximum apparent transmission was 0.773. The calculated minimum and maximum transmission coefficients (based on crystal size) are 0.5858 and 0.7531. The structure was solved using the Bruker APEX Software Package and refined with XL in Olex2, using the space group $P\bar{1}$, with Z = 2 for the formula unit, $C_{36.50}H_{35}BClF_2N_5O_3$.The final anisotropic full-matrix least-squares refinement on F^2 with 462 variables converged at R1 = 7.87%, for the observed data and wR2 = 24.36% for all data. The goodness-of-fit was 1.000. The largest peak in the final difference electron density synthesis was 0.409 $e^-/Å^3$ and the largest hole was -0.338 $e^-/Å^3$ with an RMS

deviation of 0.086 $e^-/Å^3$. On the basis of the final model, the calculated density was 1.418 g/cm^3 and F(000), 706 e^-. Refinement Note: CH_2Cl_2 disordered 50% over inversion centre. Terminal OH groups located and refined riding with restraints (DFIX). CCDC1532596 contains the supplementary crystallographic data of **9** (http://www.ccdc.cam.ac.uk/data_request/cif); see also supplementary data.

Photobleaching

Aqueous solutions of **1**, **4**, and **5** prepared by weighing **1**, **4** or **5** and transferring to a round bottom flask. For **4**, **5** anhydrous THF (10 mL) and **1** MeOH (10 mL) was added followed by 1 g of Kolliphor EL. Solutions were sonicated for 30 min, the organic solvent removed *in vacuo* and the resulting residues dried under high vacuum for 4 h. HPLC grade H_2O (10mL) was added with gentle agitation to obtain solutions which were filtered through a 0.2μm PTFE filter. Further dilution into the required volume of phenol-red free Dulbecco's modified eagle's medium (iDMEM) supplemented with 10% fetal bovine serum gave the desired fluorophore concentration. Photobleaching experiments for **1, 4** and **5** were carried by irradiating 5μM solutions of **1, 4** and **5** with 150 W fibre optic delivered white light at 25 ° C with analysis of fluorescence output over that time period.

Imaging

Aqueous solutions of **1**, **4**, and **5** prepared by weighing **1**, **4** or **5** and transferring to a round bottom flask. For **4**, **5** anhydrous THF (10 mL) and **1** MeOH (10 mL) was added followed by 1g of Kolliphor EL. Solutions were sonicated for 30 min, the organic solvent removed *in vacuo* and the resulting residues dried under high vacuum for 4 h. HPLC grade H_2O (10mL) was added with gentle agitation to obtain solutions which were filtered through a 0.2μm PTFE filter. Further dilution into the required volume of aqueous 1% w/v Kolliphor EL gave the desired fluorophore concentration.

Images taken using IVIS spectrum instrument were done so with the following settings; exposure 0.5 sec; F-stop 4; binning small; wavelengths 1: 745/800; wavelengths 2: 745/820; wavelengths 3: 745/840.

Ex vivo human tissue imaging were performed using a Novadaq PINPOINT Endoscopic system following instructions as supplied by the manufacturer.

Ethical approval

Full institutional and departmental approval within the Mater Misericordiae Hospital for the study in all aspects was granted after consideration of the study protocol.

Acknowledgements

DOS gratefully acknowledges Science Foundation Ireland grant number 11/PI/1071(T) for financial support. Thanks to Dr Brendan Twamley (Trinity College Dublin) for X-ray analysis and Mr. Kevin Conboy (University College Dublin) and Dr Gary Hessman (Trinity College Dublin) for accurate mass analysis.

Competing financial interests

A patent application has been filed on azadipyrromethene based NIR fluorophores (PCT/EP2010/065991) in which DOS has a financial interest.

Supplementary data

Supplementary data containing copies of ^{1}H and ^{13}C NMR spectra can be found at…

References

1. Vahrmeijer AL, Hutteman M, van der Vorst JR, van de Velde CJH, Frangioni, JV. Image-guided cancer surgery using near-infrared fluorescence. Nat Rev Clin Oncol 2013; 10(9): 507-518.
2. Nguyen QT, Tsien RY. Fluorescence guided surgery with live molecular navigation - a new cutting edge. Nat Rev Cancer 2013; 13(9): 655-662.
3. Liu Y, Njuguna R, Matthews T, Akers WJ, Sudlow GP, Mondal S, Tang R, Gruev V, Achilefu S. Near-infrared fluorescence goggle system with complementary metal-oxide-semiconductor imaging sensor and see-through display. Biomed Opt 2013; 18(10): 101303-7.
4. Sevick-Muraca EM. Translation of near-infrared fluorescence imaging technologies: emerging clinical applications. Annu Rev Med 2012; 63: 217-231.
5. Gioux S, Choi HS, Frangioni JV. Image-guided surgery using invisible near-infrared light: fundamentals of clinical translation. Mol Imaging 2010; 9(5): 237-255.
6. Alander JT, Kaartinen I, Laakso A, Pätilä T, Spillmann T, Tuchin VV, Venermo M, Välisuo P. A review of indocyanine green fluorescent imaging in surgery. Intern J Biomed Imaging 2012; 940585.
7. Jafari MD, Wexner SD, Martz JE, McLemore EC, Margolin DA, Sherwinter DA, Lee SW, Senagore AJ, Phelan MJ, Stamos, MJ. Perfusion assessment in laparoscopic left-sided/anterior resection (PILLAR II): a multi-institutional study. J Am Coll Surg 2015; 220(1): 82-92.
8. Liu DZ, Mathes DW, Zenn MR, Neligan PC. The application of indocyanine green fluorescence angiography in plastic surgery. J Reconstr Microsurg 2011; 27(6): 355-364.
9. Cahill RA, Anderson M, Wang LM, Lindsey I, Cunningham C, Mortensen NJ. Near-infrared (NIR) laparoscopy for intraoperative lymphatic road-mapping and sentinel node identification during definitive surgical resection of early-stage colorectal neoplasia. Surg Endosc 2012; 26(1): 197-204.
10. Toh U, Iwakuma N, Mishima M, Okabe M, Nakagawa S, Akagi Y. Navigation surgery for intraoperative sentinel lymph node detection using indocyanine green (ICG) fluorescence real-time imaging in breast cancer. Breast Cancer Res Treat 2015; 153(2): 337-344.
11. Ishizawa T, Masuda K, Urano Y, Kawaguchi Y, Satou S, Kaneko J, Hasegawa K, Shibahara J, Fukayama M, Tsuji S, Midorikawa Y, Aburatani H, Kokudo N. Mechanistic background and clinical applications of indocyanine green fluorescence imaging of hepatocellular carcinoma. Ann Surg Oncol 2014; 21(2): 440-448.
12. Cherrick GR, Stein SW, Leevy CM, Davidson CS. Indocyanine green: Observations on its physical properties, plasma decay and hepatic extraction. J Clin Invest 1960; 39: 592-600.
13. Marano A, Priora F, Matteo Lenti L, Ravazzoni F, Quarati R, Spinoglio G. Application of Fluorescence in Robotic General Surgery: Review of the Literature and State of the Art World J Surg 2013; 37: 2800-2811.

14. Grossi M, Morgunova M, Cheung S, Scholz D, Conroy E, Terrile M, Panarella A, Simpson JC, Gallagher WM, O'Shea DF. Lysosome Triggered Near Infra-Red Fluorescence; Imaging of Cellular Trafficking Processes in Real-time. Nat Commun 2016; 7: 10855. doi 10.1038/ncomms10855.
15. Wu D, Cheung S, O'Sullivan CJ, Gao Y, Chen Z, O'Shea DF. Strained Alkyne Substituted Near Infrared BF_2 Azadipyrromethene Fluorochrome. RSC Adv 2016; 6: 87373-87379.
16. Wu D, Cheung S, Devocelle M, Zhang L, Chen Z, O'Shea, DF. Synthesis and assessment of a maleimide functionalized BF_2 azadipyrromethene near-infrared fluorochrome. Chem Commun 2015; 51: 16667-16670.
17. Wu D, O'Shea DF. Synthesis and properties of BF_2-3,3'-dimethyldiaryl azadipyrromethene near-infrared fluorophores. Org Lett 2013; 15: 3392-3395.
18. Ge Y, O'Shea DF. Azadipyrromethenes: From Traditional Dye Chemistry to Leading Edge Applications. Chem Soc Rev 2016; 45: 3846-3864.
19. Rurack K, Spieles, M. Fluorescence Quantum Yields of a Series of Red and Near-Infrared Dyes Emitting at 600-1000 nm. Anal Chem 2011; 83: 1232-1242.
20. Gioux S, Choi HS, Frangioni JV. Image-Guided Surgery Using Invisible Near-Infrared Light: Fundamentals of Clinical Translation. Mol Imag 2010; 9(5): 237-255.
21. Loudet A, Bandichhor R, Burgess K, Palma A, McDonnell SO, Hall MJ, O'Shea DF B,O-chelated azadipyrromethenes as near-IR probes. Org Lett 2008; 21: 4771-4774.
22. Zhao W, Carreira EM. Conformationally Restricted Aza-BODIPY: Highly Fluorescent, Stable Near-Infrared Absorbing Dyes. Chem Eur J 2006; 12: 7254-7263.
23. Wu Y, Cheng C, Jiao L, Yu C, Wang S, Wei Y, Mu X, Hao E. Org Lett 2014; 16: 748-751.
24. McDonnell SO, O'Shea DF. Near infrared sensing properties of dimethlyamino substituted BF_2-azadipyrromethenes. Org Lett 2006; 8: 3493-3496.
25. Jin T, Tsuboi S, Komatsuzaki A, Imamura Y, Muranaka Y, Sakata T, Yasuda H. Enhancement of aqueous stability and fluorescence brightness of indocyanine green using small calix[4]arene micelles for near-infrared fluorescence imaging. Med Chem Commun 2016; 7: 623-631.
26. Gelderblom H, Verweij J, Nooter K, Sparreboom A. Cremophor EL: the drawbacks and advantages of vehicle selection for drug formulation. Eur J Cancer 2001; 37: 1590-1598.
27. Gu K, Xu Y, Li H, Guo Z, Zhu S, Zhu S, Shi P, James TD, Tian H, Zhu W-H. Real-time tracking and in vivo visualization of β-galactosidase activity in colorectal tumor with a ratiometric near-infrared fluorescent probe. J Am Chem Soc 2016; 138: 5334-5340.
28. X Acuna SA, Elmi M, Shah PS, Coburn NG, Quereshy FA. Preoperative localization of colorectal cancer: a systematic review and meta-analysis. Surg Endosc 2016; Oct 3; epub ahead of print PMID: 27699516.
29. Watanabe M, Tsunoda A, Narita K, Kusano M, Miwa M. Colonic Tattooing Using Fluorescence Imaging with Light-Emitting Diode-Activated Indocyanine Green: A Feasibility Study. Surg Today 2009; 39: 214-218.
30. Ong, MLH, Schofield, JB. Assessment of lymph node involvement in colorectal cancer. World J Gastrointest Surg 2016; 8(3): 179-192.

31. Cahill RA, Bembenek A, Sirop S, Waterhouse DF, Schneider W, Leroy J, Wiese D, Beutler T, Bilchik A, Saha S, Schlag PM. Sentinel node biopsy for the individualization of surgical strategy for cure of early-stage colon cancer. Ann Surg Oncol 2009; 16(8): 2170-80.
32. Hutteman M, Choi HS, Mieog JSD, van der Vorst JR, Ashitate Y, Kuppen PJK, van Groningen MC, Löwik CWGM, Smit VTHBM, van de Velde CJH, Frangioni JV, Vahrmeijer, AL. Clinical translation of ex vivo sentinel lymph node mapping for colorectal cancer using invisible near-infrared fluorescence light. Ann Surg Oncol 2011; 18: 1006-1014.
33. In our hands this *ex vivo* experimental method was inconsistent as migration through the lymphatics occurred infrequently with more often the fluorophore remaining visible only at the site of injection.